The Angular Distribution of Auroral Kilometric Radiation

JAMES LAUER GREEN, DONALD A. GURNETT, AND STANLEY D. SHAWHAN

Department of Physics and Astronomy, University of Iowa, Iowa City, Iowa 52242

Measurements of the angular distribution of auroral kilometric radiation (AKR) are presented by using observations from the Hawkeye 1, Imp 6, and Imp 8 satellites. The University of Iowa plasma wave experiments on Hawkeye 1 and Imp 6 provide electric field measurements of AKR in narrow frequency bands centered at 178, 100, and 56.2 kHz, and the Imp 8 experiment provides measurements at 500 kHz. From a frequency of occurrence survey, at radial distances greater than 7 R_E (earth radii) it is shown that AKR is preferentially and instantaneously beamed into solid angles of approximately 3.5 sr at 178 kHz, 1.8 sr at 100 kHz, and 1.1 sr at 56.2 kHz, directed upward from the nighttime auroral zones. Simultaneous multiple satellite observations of AKR in the northern hemisphere show that the radiation occurs simultaneously throughout these solid angles and that the plasmapause acts as an abrupt propagation cutoff on the nightside of the earth. No comparable cutoff is observed at the plasmapause on the dayside of the earth.

The results of computer ray tracing calculations for both the right-hand (*R-X*) and left-hand (*L-O*) polarized modes are also presented in an attempt to understand the propagation characteristics of the AKR. These calculations assume that a small source emits radiation at various frequencies along a magnetic field line at 70° invariant latitude near local midnight. The approximate altitude of the source can be determined for each of the two modes of propagation by adjusting the source altitude to give the best fit to the observed angular distributions. The *R-X* mode is found to give the best agreement with the observed angular distributions.

INTRODUCTION

Recent satellite observations have revealed two distinctly different nonthermal radio emissions associated with the earth's magnetosphere. Both types of emissions occur at kilometric wavelengths in the radio spectrum. One of these types of radiation has a relatively constant intensity and is very weak. This radiation has been called the 'nonthermal continuum' and is generated between the plasmapause and the magnetopause, the greatest intensity being on the dayside of the earth [*Gurnett*, 1975]. The other type of radiation, which has been called 'terrestrial kilometric radiation' by *Gurnett* [1974] and by *Kaiser and Alexander* [1976], consists of intense sporadic bursts of electromagnetic radiation generated over a wide range of distances (2–15 R_E) above the auroral zones [*Kaiser and Alexander*, 1976]. Since the most intense and frequently occurring kilometric radio emissions originate from the nighttime auroral regions and are closely correlated with the occurrence of aurora, *Kurth et al.* [1975] have called these emissions 'auroral kilometric radiation.' The present study only considers satellite observations of auroral kilometric radiation (AKR).

Dunckel et al. [1970] first showed that AKR was correlated with the auroral electrojet index *AE*. Using photographs produced from the optical scanner aboard the Dapp satellite, *Gurnett* [1974] demonstrated a close association of AKR with discrete auroral arcs. Since *Ackerson and Frank* [1972] had previously showed that intense 'inverted V' electron precipitation events are correlated with discrete auroral arcs, *Gurnett* [1974] concluded that AKR is closely associated with the inverted V electron precipitation.

The power spectrum of AKR has a large degree of variability with time. *Gurnett* [1974] presented a power spectrum of a typical auroral kilometric burst as observed by Imp 8 that had a peak power flux of about 10^{-14} W m^{-2} Hz^{-1} at 178 kHz. On either side of the peak the spectrum decreased rapidly in intensity, decreasing to the receiver noise level at about 30 kHz and to near the cosmic background at 2 MHz. *Kaiser and Stone* [1975] presented a similar power spectrum with peak frequency near 500 kHz, and they also indicated that the peak may sometimes be as low as 130 kHz. *Gurnett* [1974] estimated that at peak intensity the total power of AKR is sometimes as high as 10^9 W.

Preliminary evidence presented by *Gurnett* [1974] at 178 kHz indicated that AKR is generated at radial distances as low as 2.8 R_E (earth radii) in the evening auroral zone from a source that 'subtends a small angular size.' Direction finding measurements from Imp 8 and Hawkeye 1 were used by *Kurth et al.* [1975] to locate the average source region of AKR projected onto the equatorial plane at the frequency of 178 kHz. From Imp 8 observations the average source region was found to be at a local time of 21.25 hours and at a distance of 0.835 R_E from the polar axis. These measurements would place the source at a geocentric radial distance of about 2 R_E along an auroral field line (70° invariant latitude). The Hawkeye 1 observations presented by *Kurth et al.* [1975] also gave similar results.

Using RAE 2 in orbit about the moon, *Kaiser and Alexander* [1976] produced two-dimensional source location measurements of AKR from lunar occultations. They found that although the average source location at 250 kHz is between 2 and 3 R_E above the polar regions, a number of events indicated that the radiation may occasionally be generated at large radial distance (>7 R_E). From single lunar occultations, *Alexander and Kaiser* [1976] have observed several source regions at the same frequency. The most intense component of the multiple sources is almost always closest to the earth, and the weakest component is the most distant. A preliminary investigation by *Alexander and Kaiser* [1976] of the variation of source positions with observing frequency indicated that AKR emission at frequencies above 300 kHz came from closer to the earth than the emissions at frequencies less than 250 kHz. In addition, the sources in the northern hemisphere, on the nightside, appear to trace out a 70° invariant latitude magnetic field line.

The purpose of this paper is to determine the angular distribution of auroral kilometric radiation at different frequencies

Paper number 7A0137.

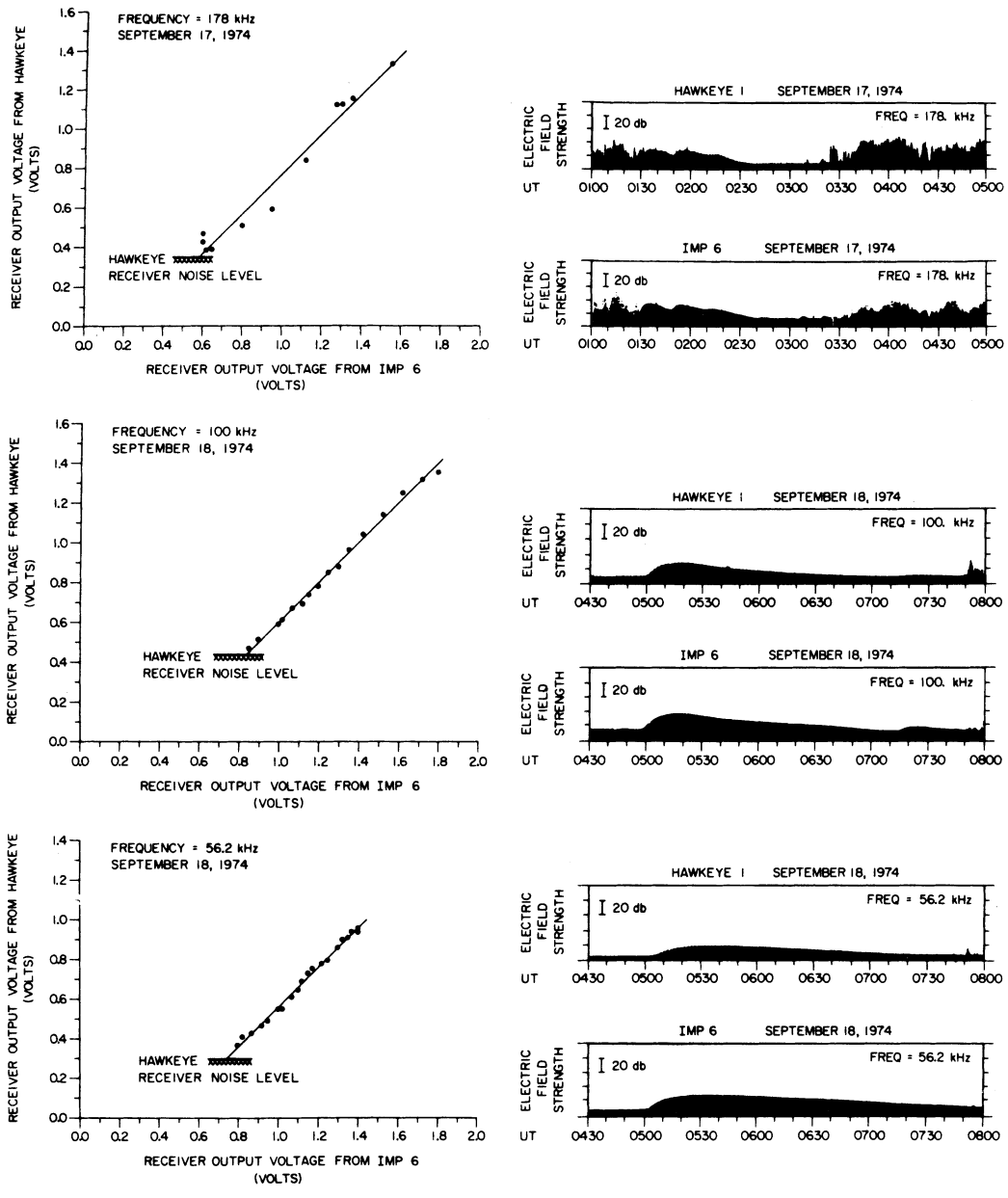

Fig. 1. Cross calibration of the receiver responses of the plasma wave experiments on Hawkeye 1 and Imp 6 using simultaneous observations of a type III radio burst.

by making use of observations from three satellites over a period of several years. Variations in these observed angular distributions as a function of frequency are then explored by using ray tracing calculations in order to obtain more information on the spatial position and characteristics of the source region of AKR. The ray tracing calculations also indicate the most probable polarization of this electromagnetic radiation.

Method of Analysis

Instrumentation

The University of Iowa has nearly identical plasma wave experiments on board Hawkeye 1, Imp 6, and Imp 8. Imp 6 and Hawkeye 1 are in highly elliptical earth orbits. The apogee of Hawkeye 1 is over the north polar region at a radial distance of 130,856 km. The apogee of Imp 6 is near the equatorial plane (orbit inclination of 28.7°) at a radial distance of 212,630 km. Imp 8 is in a low-eccentricity earth orbit near the equatorial plane with initial perigee and apogee radial distances of 147,434 and 295,054 km, respectively, and an orbit inclination of 28.6°.

Each of the three satellites has a long dipole antenna for electric field measurements. The Hawkeye 1 antenna is the shortest, measuring 42.45 m from tip to tip. The Imp 6 and Imp 8 antennae are longer, 92.5 and 121.8 m from tip to tip, respectively. To determine the electric field intensity at various frequencies, the antenna signals are periodically analyzed with spectrum analyzers. The Imp 6 spectrum analyzer has 16 frequency bands with center frequencies from 36 Hz to 178 kHz. For this experiment the filter bandwidths range from about ±10% of the center frequency at high frequencies to ±20% at low frequencies. The electric field spectrum analyzers on board Hawkeye 1 and Imp 8 also have 16 narrow band frequency channels with center frequencies from 1.78 Hz to 178 kHz (±10%) and 40 Hz to 178 kHz (±10%), respectively. In addition, Imp 8 has a tunable wide band receiver which measures

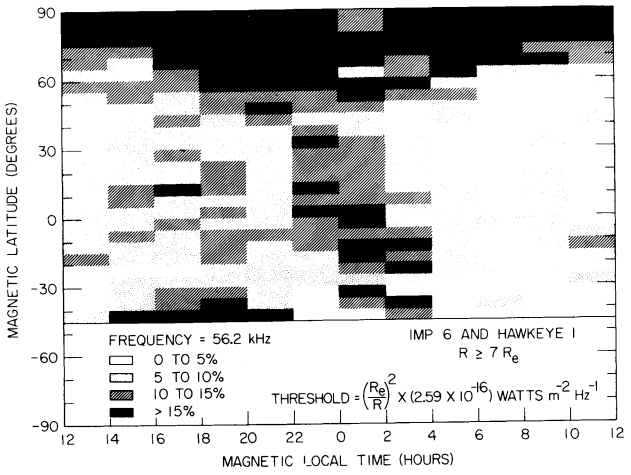

Fig. 2. The frequency of occurrence diagram of AKR as observed from the Imp 6 and Hawkeye 1 spacecraft at 56.2 kHz as a function of MLT and magnetic latitude.

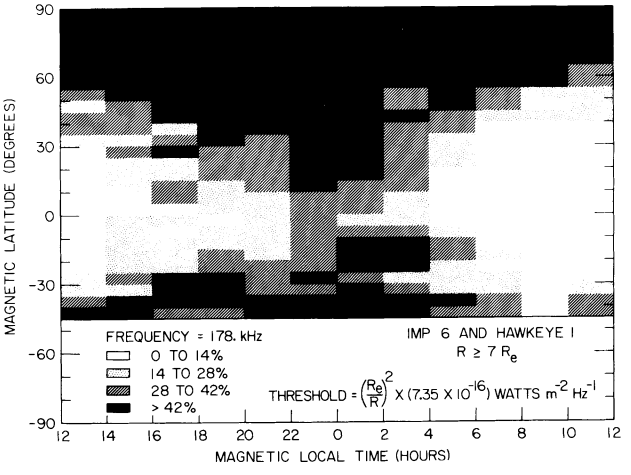

Fig. 4. The frequency of occurrence diagram of AKR as observed from the Imp 6 and Hawkeye 1 spacecraft at 178 kHz as a function of MLT and magnetic latitude.

the electric field intensity at 2 MHz, 500 kHz, 125 kHz, or 31.1 kHz with a bandwidth of ±1 kHz. The dynamic range of each of these instruments is about 100 dB. The raw data from the spectrum analyzer channels are transmitted as voltages which range from 0 to 5 V and are approximately proportional to the logarithm of the electric field intensity.

In 6 months, Hawkeye 1 covers 24 hours of magnetic local time and provides observations over essentially the entire northern polar regions. Complete coverage of magnetic latitudes between −45° and +45° at all magnetic local times (out to 33 R_E) is accomplished by Imp 6 after 1 year in orbit. The magnetic latitudinal coverage of Imp 6 and Imp 8 is quite similar, but a larger body of data is now available from Imp 6. Consequently, observations from Imp 6 and Hawkeye 1 will be combined to determine the angular extent of AKR at 56.2, 100, and 178 kHz in the northern hemisphere. Additional coverage by Imp 8 at 500 kHz is also presented to extend the analysis to higher frequencies.

Cross Calibration of Hawkeye 1 and Imp 6

Since data from two different satellites, Imp 6 and Hawkeye 1, are to be combined in a single frequency of occurrence analysis, it is necessary to perform a cross calibration of the two instrument sensitivities to make certain that no systematic differences are present in the calibrations. A convenient method of performing such a cross calibration is to compare simultaneous observations of a type III solar radio burst. Type III bursts are radio emissions from superthermal electrons emitted by the sun during a flare [*Lin*, 1970]. The use of the type III bursts to provide a cross calibration of Hawkeye 1 and Imp 6 is based on the assumption that the distance between the satellites is small compared to the distance the radiation has to travel from the source to the two satellites. Both satellites are then subjected to the same power flux.

Figure 1 shows a series of simultaneous observations of type III solar radio bursts by Imp 6 and Hawkeye 1 at 56.2 and 100 kHz on September 18, 1974, and at 178 kHz on September 17, 1974. The signature of the type III burst at these frequencies can be recognized easily by the smooth rapid increase in signal strength to a maximum on a time scale of a few minutes followed by a gradual decrease to the receiver noise level on a time scale of several tens of minutes. Note the multiple type III event on September 17, 1974, in the 178-kHz channels. The large sporadic intensity fluctuations on either side of the multiple type III events in Figure 1 are bursts of AKR. Close

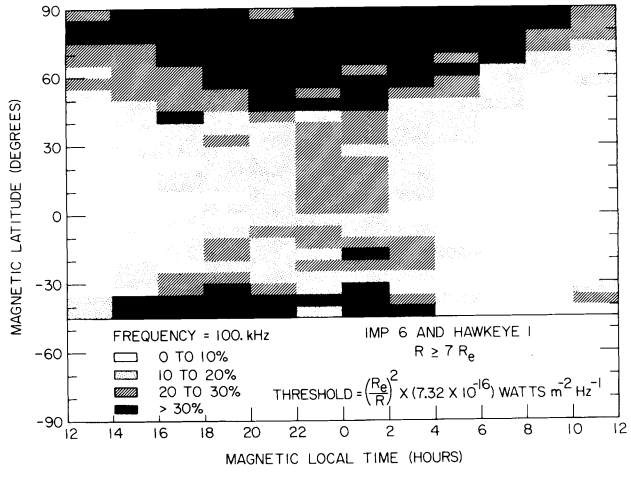

Fig. 3. The frequency of occurrence diagram of AKR as observed from the Imp 6 and Hawkeye 1 spacecraft at 100 kHz as a function of MLT and magnetic latitude.

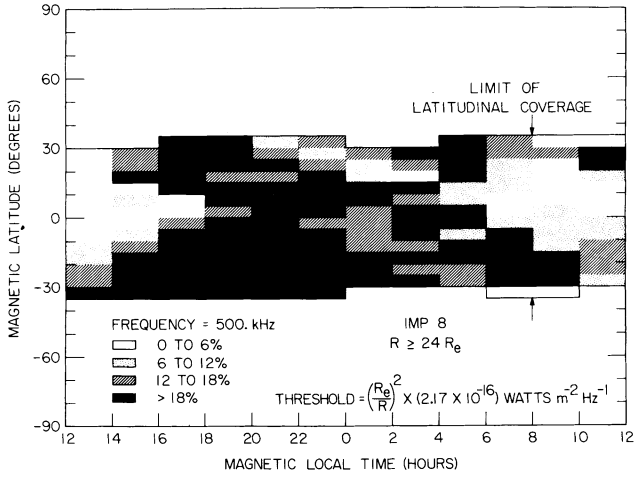

Fig. 5. The frequency of occurrence diagram of AKR as observed from the Imp 8 spacecraft at 500 kHz as a function of MLT and magnetic latitude.

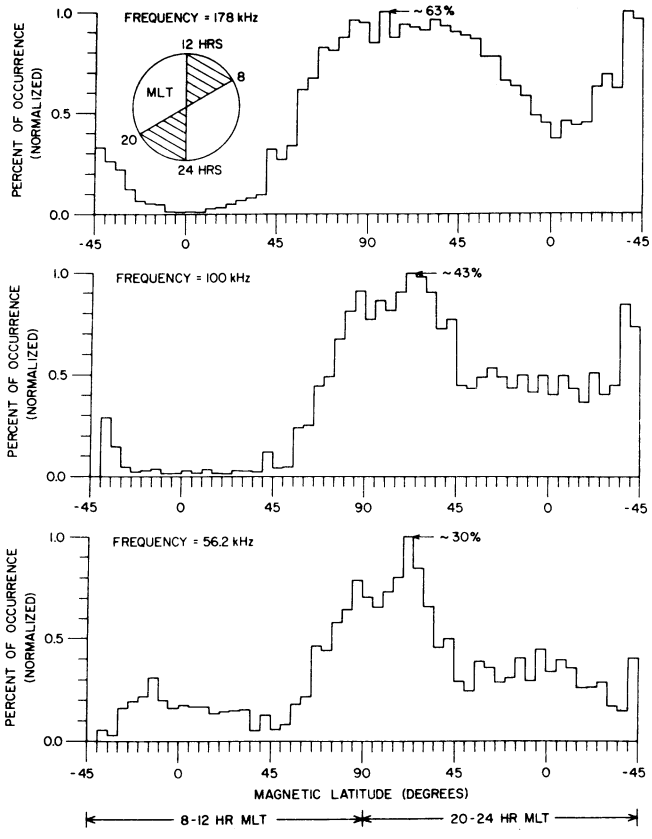

Fig. 6. The normalized percentage of occurrence of AKR in magnetic meridian sections between 8 and 12 hours and 20 and 24 hours MLT.

examination shows that both satellites are receiving the same AKR bursts, as is evident by the closely correlated variation of the electric field strengths in the 178-kHz channels.

The cross calibration graphs on the left of Figure 1 are obtained by plotting the raw voltage output of the Hawkeye spectrum analyzer versus the raw voltage output of the Imp 6 analyzer for these type III bursts. Each point is a measurement from both satellites taken at the same time and at the same frequency during the slowly decreasing part of the type III radio burst. Only the peak intensities were used in these comparisons to take into account any spin modulation effects. From the straight line fits in each graph the relationship between the output voltage from the receivers on Hawkeye 1 and Imp 6 can be found. In every case the slope of each straight line fit is one, confirming that the sensitivities of the receivers are identical. The absolute magnitudes of the intensities determined from the preflight calibrations agree within 2 dB.

The Observed Angular Distribution

Information on the angular distribution of AKR can be obtained by examining where the satellites have observed the highest frequency of occurrence of radiation above a preset threshold. A two-dimensional frequency of occurrence diagram of AKR can be constructed in magnetic latitude (λ_m) and magnetic local time (MLT) by using a $1/R^2$ power flux threshold criterion to correct for the expected $1/R^2$ radial variations of the power flux [see *Gurnett*, 1974]. Although the source is not located at the center of the earth, this radial variation corrects for the first-order radial dependence of the power flux, provided the source is located relatively close to the earth.

On the basis of a survey of 10 months of Hawkeye 1 data at 178, 100, and 56.2 kHz and 1½ years of Imp 8 data at 500 kHz a power flux threshold was chosen 25 dB below the maximum power flux observed for each frequency. This threshold was a compromise resulting from the conflicting requirements to obtain enough data points above the threshold for good statistical accuracy, and at the same time assure that the threshold is well above the receiver noise for each spacecraft and for each frequency analyzed. The thresholds selected are as follows:

$$(500\text{ kHz})\text{ threshold} = (R_E/R)^2 \times (2.17 \times 10^{-16})\text{ W m}^{-2}\text{ Hz}^{-1}$$
$$(178\text{ kHz})\text{ threshold} = (R_E/R)^2 \times (7.35 \times 10^{-16})\text{ W m}^{-2}\text{ Hz}^{-1}$$
$$(100\text{ kHz})\text{ threshold} = (R_E/R)^2 \times (7.32 \times 10^{-16})\text{ W m}^{-2}\text{ Hz}^{-1}$$
$$(56.2\text{ kHz})\text{ threshold} = (R_E/R)^2 \times (2.59 \times 10^{-16})\text{ W m}^{-2}\text{ Hz}^{-1}$$

Since the distance from the spacecraft to the source of AKR is not known during the initial reduction of data, the R value used in calculating the power flux threshold is the geocentric radial distance to the spacecraft. To reduce the error caused by the uncertainty in the radial distance to the source and to avoid complications due to near-earth propagation effects, only measurements obtained at $R > 7\ R_E$ are used in the analysis. If the source is near the earth ($R < 3\ R_E$), then the margin of error in the radial distance correction of the threshold is at most ±4 dB, which is small in comparison with the amplitude range (~100 dB) over which the intensity of AKR varies.

The frequency of occurrence diagram determined from the frequency of occurrence analysis for 56.2 kHz is shown in Figure 2. The measurements used comprise 3.5 years of Imp 6 data and 10 months of Hawkeye 1 data. Blocks of 5° increments in λ_m and 2-hour increments of MLT are used. The magnetic coordinates of the spacecraft determine the block within which an observation is counted. In each block the total number of 3-min observations of AKR above the threshold are counted. This number is divided by the total number of 3-min observations in that block to give the frequency of occurrence. The black shading in Figure 2 represents the highest percentage of times that AKR was detected above the power flux threshold. The distinct emission cone (black shading) of AKR is clearly evident in Figure 2 in the northern hemisphere. The emission cone appears to be completely filled and is symmetric, centering around 22 hours MLT, indicating that the preferred direction of AKR is in the local evening, in agreement with direction finding measurements of the average source locations by *Kurth et al.* [1975] and *Kaiser and Stone* [1975]. Near local midnight the latitudinal boundary of the emission cone extends to near the magnetic equator and is rather poorly defined, as is indicated by the complicated variations of the frequency of occurrence in this region. At high magnetic latitudes on the dayside of the earth (6–10 hours MLT) the frequency of occurrence of AKR changes by at least a factor of 4 at $\lambda_m = 65° \pm 10°$. This rapid change in the frequency of occurrence indicates that a relatively stable boundary to the AKR angular distribution occurs on the dayside of the earth.

The frequency of occurrence diagrams at 100 and 178 kHz, shown in Figures 3 and 4, respectively, were produced in the same manner as those of Figure 2. AKR is observed with

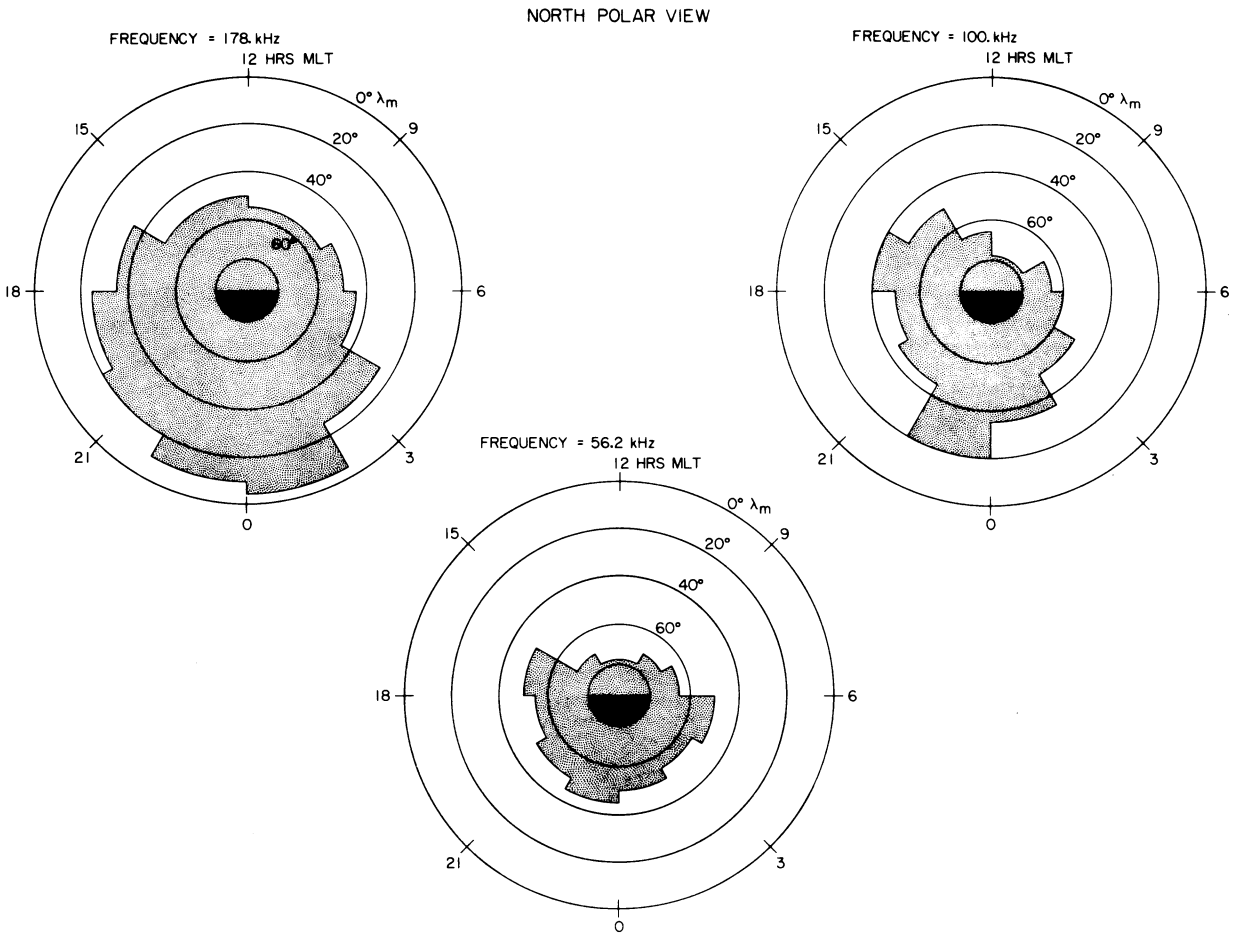

Fig. 7. A north polar view of the latitudinal boundary of the AKR emission cones at 178, 100, and 56.2 kHz in magnetic coordinates. The decreasing angular size of the emission region with decreasing frequency is clearly evident.

almost equal frequency throughout the emission cones (black shading) at 100 kHz and 178 kHz. Similarities with Figure 2 include (1) a rapid change in the frequency of occurrence at high λ_m on the dayside of the earth, (2) a complicated poorly defined latitudinal boundary at low latitudes on the nightside of the earth, and (3) symmetry about 22 hours MLT. At higher frequencies (particularly 178 kHz) the emission cones extend closer to the magnetic equator in the local evening.

Figure 5 shows the frequency of occurrence of AKR at 500 kHz from 1½ years of Imp 8 data. Hawkeye 1 and Imp 6 do not have a 500-kHz channel, and consequently we are limited in latitudinal coverage to $\pm 45°$ λ_m. Figures 2, 3, 4, and 5 are consistent with the general picture that from 56.2 to 500 kHz the solid angle of the emission cones increases as the frequency increases. At 500 kHz the northern and southern emission cones appear to overlap substantially in the region near local midnight.

To obtain a better impression of the latitudinal variation of the frequency of occurrence, we can normalize each of these frequency of occurrence diagrams. The normalization is accomplished by changing the scale of each frequency of occurrence diagram to a scale that ranges from zero to one where the maximum percentage of occurrence equals one. Figure 6 shows the normalized percentage of observed AKR for the three frequencies 178, 100, and 56.2 kHz versus magnetic latitude. All observations on the dayside of the earth with MLT between 8 and 12 hours are on the left side of each panel. The right side shows observations on the nightside of the earth from 20 to 24 hours MLT. The observations are organized by magnetic latitude, the north magnetic pole being located directly at the center of each plot. Starting at the pole, the normalized occurrence decreases rapidly with decreasing latitude on the dayside of the earth, with a sharp boundary at about $\lambda_m = 65° \pm 10°$ for all frequencies. On the nightside of the earth the normalized occurrence decreases less rapidly with decreasing latitude and has a nearly constant plateau from about $+45°$ to $-45°$ in the 56.2- and 100-kHz channels. The 178-kHz distribution extends closer to the equator than the 100- and 56.2-kHz distribution. The day-night skewness in the normalized occurrence of AKR evident in Figure 6 could be produced by an angular distribution that would be variable in time on the nightside of the earth and spatially fixed in time on the dayside.

A north polar view of the angular distribution of AKR can be constructed by noting the magnetic latitude of the normalized half-occurrence points at all MLT. The boundaries of the shaded areas in Figure 7 show the position of these normalized half-occurrence points in magnetic coordinates. This illustration shows that AKR is preferentially beamed into larger solid angles at higher frequencies, approximately 1.1 sr at 56.2 kHz,

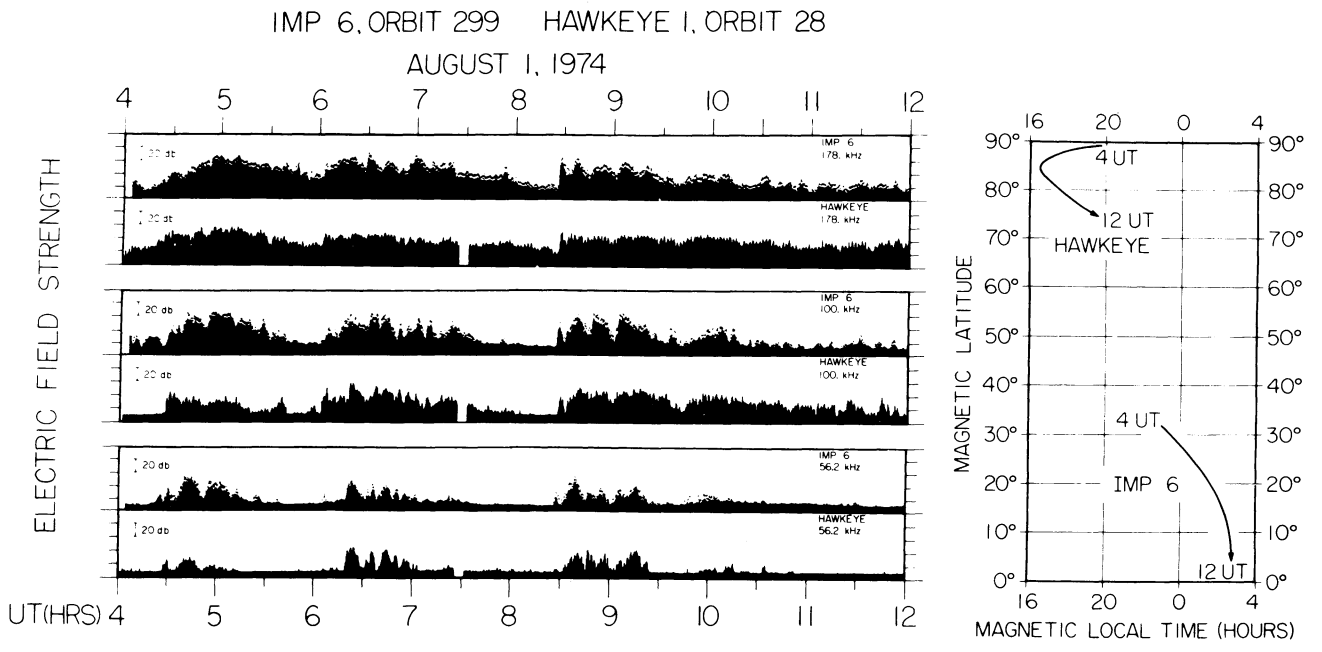

Fig. 8. Simultaneous observations from the Hawkeye 1 and Imp 6 spacecraft of AKR at widely separated magnetic latitudes. In this case the intensity variations are closely correlated, indicating that the radiation occurs simultaneously over a large solid angle. In addition, the absolute power fluxes are approximately the same at both spacecraft.

1.8 sr at 100 kHz, and 3.5 sr at 178 kHz. On the assumption that the angular distribution at 500 kHz is completely filled in over the polar regions, Figure 5 shows that the solid angle at 500 kHz is approximately 5.3 sr, in agreement with the general trend toward larger solid angles at higher frequencies.

Simultaneous Observations at Widely Separated Locations

Simultaneous observations from two satellites at widely separated locations reveal many important characteristics of AKR that cannot be discerned with a single satellite. One of the most important questions which can be investigated is whether or not individual bursts of AKR simultaneously and uniformly illuminate the large solid angles depicted in Figure 7 or whether these frequency of occurrence distributions could be the result of a much narrower instantaneous beam or cone which varies in time.

To illustrate, Figure 8 presents simultaneous electric field data from Imp 6 and Hawkeye 1 for the same auroral kilometric storms. On the left side of this figure the corresponding frequencies from each satellite are individually compared in plots of electric field intensity versus time. It is easy to see that both satellites are observing radiation originating from the same source. On the right side the satellite trajectories are shown in MLT and λ_m coordinates for the corresponding time period. Figure 8 illustrates that individual AKR bursts radiate into large solid angles and that the frequency of occurrence diagrams are not representations of small solid angle beams of AKR that have moved in time. In addition, the absolute power fluxes of AKR observed by both satellites are nearly identical (to within about 2 dB). This important observation indicates that the source of AKR uniformly illuminates the entire region within the emission cones.

Simultaneous observations of electric field data from Imp 8 and Hawkeye 1 can be used to investigate propagation cutoff characteristics of AKR. In Figure 9, for instance, Imp 8 is near 3 hours MLT at large radial distances and is observing intense storms of AKR during the entire time period shown. Hawkeye 1 also observes these intense storms of AKR but only in certain regions of its orbit. This is evidently a spatial effect and not a temporal effect, since Imp 8 still observes AKR when Hawkeye 1 is not detecting the radiation.

The position of the plasmapause in Figure 9 has been identified by the change in the low-frequency (17.8 Hz) electric field intensity and the plasmaspheric hiss cutoff, similar to the observations of *Shaw and Gurnett* [1975]. The identification of the upper hybrid resonance (UHR) noise in Figure 9 also provides an indication of the location of the plasmapause boundary. As is evident in Figure 9, the position of the plasmapause at 1152 UT (universal time) closely corresponds to the abrupt drop in intensity of AKR as observed from Hawkeye 1 near local midnight. The times of the signal loss for the different frequencies (178, 100, and 56.2 kHz) are not the same. At higher frequencies the propagation cutoff tends to occur closer to the earth. This propagation cutoff characteristic of AKR at low altitudes on the nightside has been previously reported by *Gurnett* [1974] from Imp 6 data and is assumed to occur when the local electron plasma frequency exceeds the wave frequency. *Gurnett* [1974] notes that the propagation cutoffs of AKR are consistent with the expected rapid increase in the plasma density, and hence plasma frequency, at the plasmapause. These observations imply that the extent of the propagation of AKR on the nightside is limited by the local plasma characteristics at the plasmapause.

At 1403 UT in Figure 9, Hawkeye 1 again leaves the plasmapause, but it is now on the dayside of the earth. As the spacecraft travels upward in its trajectory, the intensity of the AKR gradually begins to increase over a distance of several earth radii and does not exhibit a sharp propagation cutoff such as was observed on the nightside of the earth. Imp 8 meanwhile observes many large amplitude bursts of AKR at its position on the nightside, confirming that AKR is present

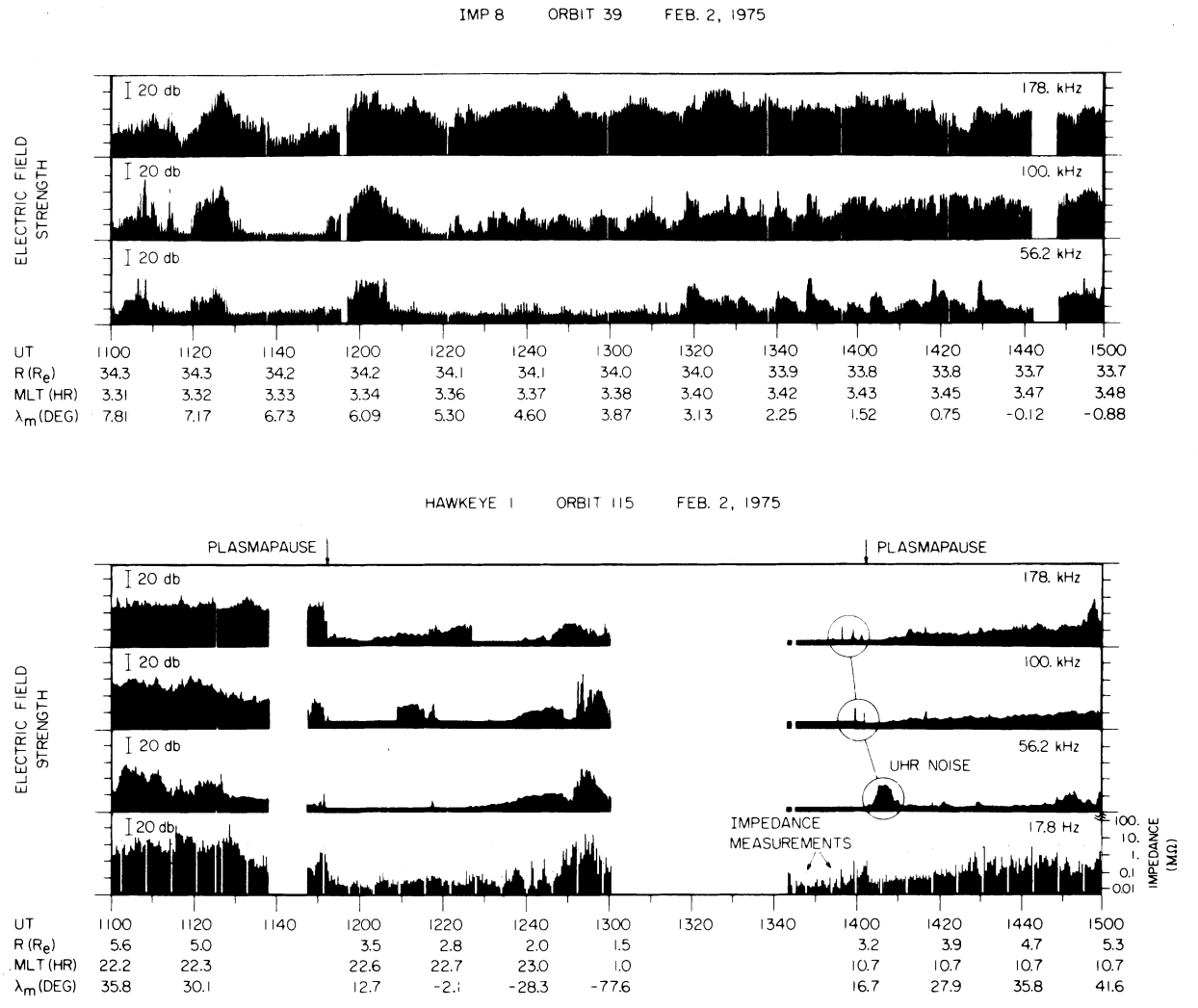

Fig. 9. Simultaneous observations from Imp 8 and Hawkeye 1. Imp 8 is at large radial distances on the nightside in the northern hemisphere observing intense bursts of AKR. Meanwhile, Hawkeye 1 moves in and out of the emission cones of AKR as it passes through the inner regions of the earth's magnetosphere near the noon-midnight meridian. As observed from Hawkeye 1, the plasmapause acts as an abrupt propagation cutoff to AKR only on the nightside. On the dayside, AKR does not propagate down to the plasmapause. The 17.8-Hz channel is used to determine the position of the plasmapause.

during this period. The absence of an abrupt propagation cutoff indicates that the latitudinal boundary of the illumination region on the dayside of the earth is not determined by the plasma characteristics near the plasmapause, in direct contrast with what is observed on the nightside. This asymmetry in the angular distribution in the noon-midnight meridian provides important information about the propagation of AKR at low altitudes (3–5 R_E). Any meaningful model of AKR ray paths must describe this effect.

Comparison of Computed Ray Paths With Observed Angular Distributions

Introduction

From cold plasma theory it is known that the only modes which can escape into 'free space' (where the magnetic field and plasma density are small compared to the source region) are the right-hand polarized extraordinary (*R-X*) mode and the left-hand polarized ordinary (*L-O*) mode. Mechanisms which lead to radiation primarily in the left-hand mode have been proposed by *Benson* [1975], *Palmadesso et al.* [1976], and *Jones* [1976]. Right-hand polarized radiation will be produced by the generation mechanisms proposed by *Scarf* [1974], *Gurnett* [1974], and *Melrose* [1976]. In addition, *Barbosa* [1976] suggests a process which produces both *R-X* and *L-O* components. At the present time there is no direct experimental evidence on the polarization of AKR or the exact height at which the radiation is generated.

Ray tracing calculations can be used in comparisons with the observed angular distributions to provide information on the polarization of AKR and on the region in which the radiation is generated. It will be shown from such comparisons that the ray paths are very sensitive to the source location and to the polarization.

The Electron Density and Magnetic Field Models

In order for a valid comparison to be made the magnetospheric models which are used in the ray tracing must be acceptable representations of the physical environment that

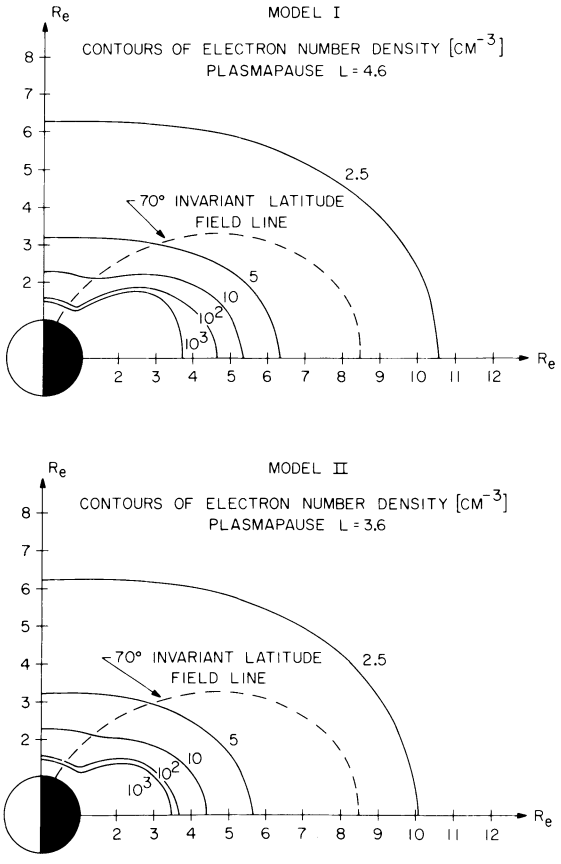

Fig. 10. Two model magnetospheres used in the ray tracing of AKR. The main difference between the models is the size of the plasmapause. Model I has a plasmapause L value of 4.6 and represents the earth's magnetosphere in times of moderate geomagnetic activity. Model II has a plasmapause L value of 3.6 for times of severe geomagnetic activity. Only the electron distributions in the northern hemisphere on the nightside are shown in this figure.

influences the radiation. The polar magnetosphere and plasmapause are known to be strongly dependent on geomagnetic activity. AKR is observed most frequently during times of disturbed geomagnetic activity [*Dunckel et al.*, 1970; *Gurnett*, 1974; *Voots et al.*, 1976]. Since the plasmapause position plays an important role in controlling the angular extent of the AKR on the nightside of the earth, it is important that a suitable model of the plasmapause position be used. During moderate magnetic activity the plasmapause is located at about 4.5 R_E geocentric radial distance in the equatorial plane near local evening [*Carpenter*, 1963]. At times of severe magnetic storms the plasmapause contracts inward to about 3.5 R_E [*Carpenter*, 1963]. The plasmapause is believed to be closely aligned along the magnetic field.

For these ray tracing studies, two models, shown in Figure 10, have been used for the electron density near the plasmapause. For model I the plasmapause is located at $L = 4.6$, and for model II the plasmapause is at $L = 3.6$. For both models the electron density is 100 cm^{-3} at the plasmapause. In all cases it is assumed that the radio emission is generated along a magnetic field line which intersects the earth at 70° invariant latitude ($L = 8.55$). Since the earth's magnetic field closely resembles a dipole field at the relatively low altitudes where the AKR is believed to be generated, an ideal dipole field is used with a surface magnetic field strength of 0.62 G at the poles. The electron density is assumed to decrease very rapidly with increasing radial distance over the polar regions, reaching a density of about 10 cm^{-3} at 2.25 R_E (essentially the modified polar wind model used by *Gurnett* [1974]).

Experimental justification for some of the main features of the density contours in models I and II can be found in Figure 9. The UHR noise band in Figure 9 has a frequency range that extends between the local plasma frequency and the local UHR frequency [*Shaw and Gurnett*, 1975]. From the plasmapause determined by the peak in the 17.8-Hz channel and the

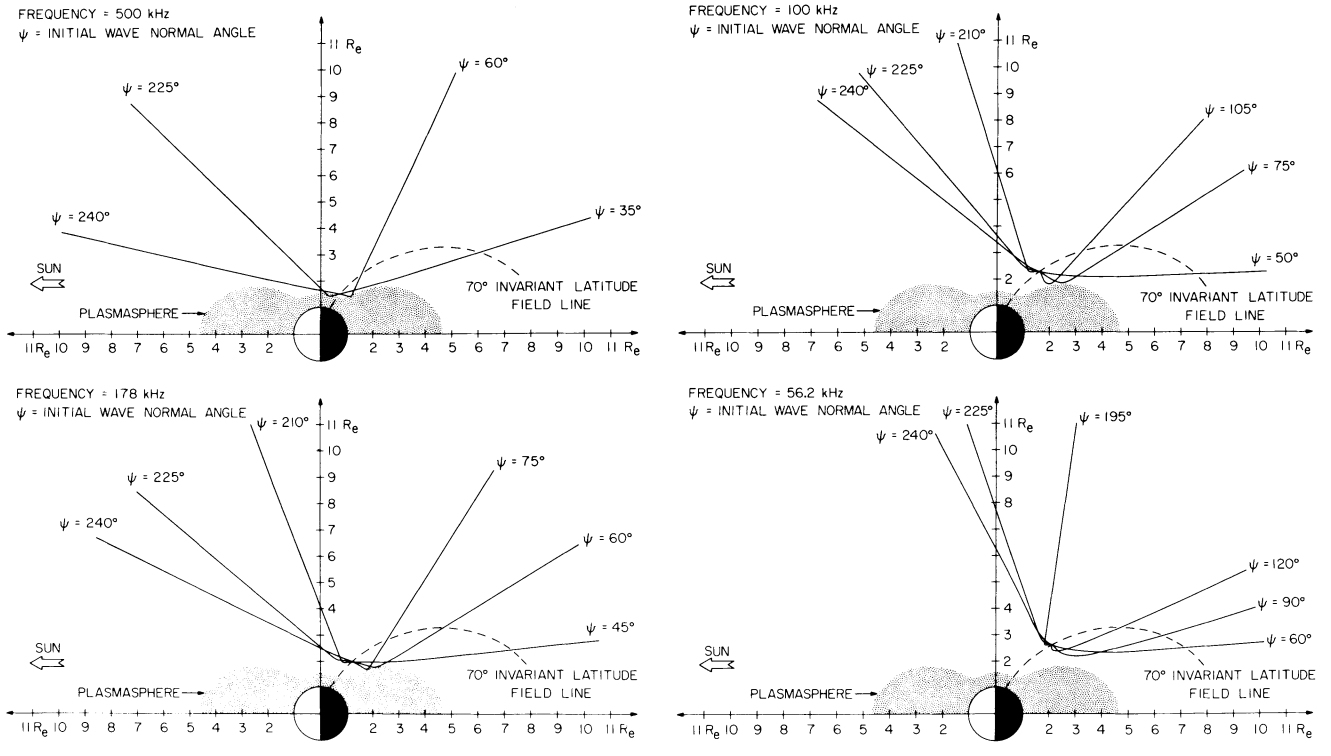

Fig. 11. Ray tracing examples of radiation in the R-X mode in the model I magnetosphere at 500, 178, 100, and 56.2 kHz.

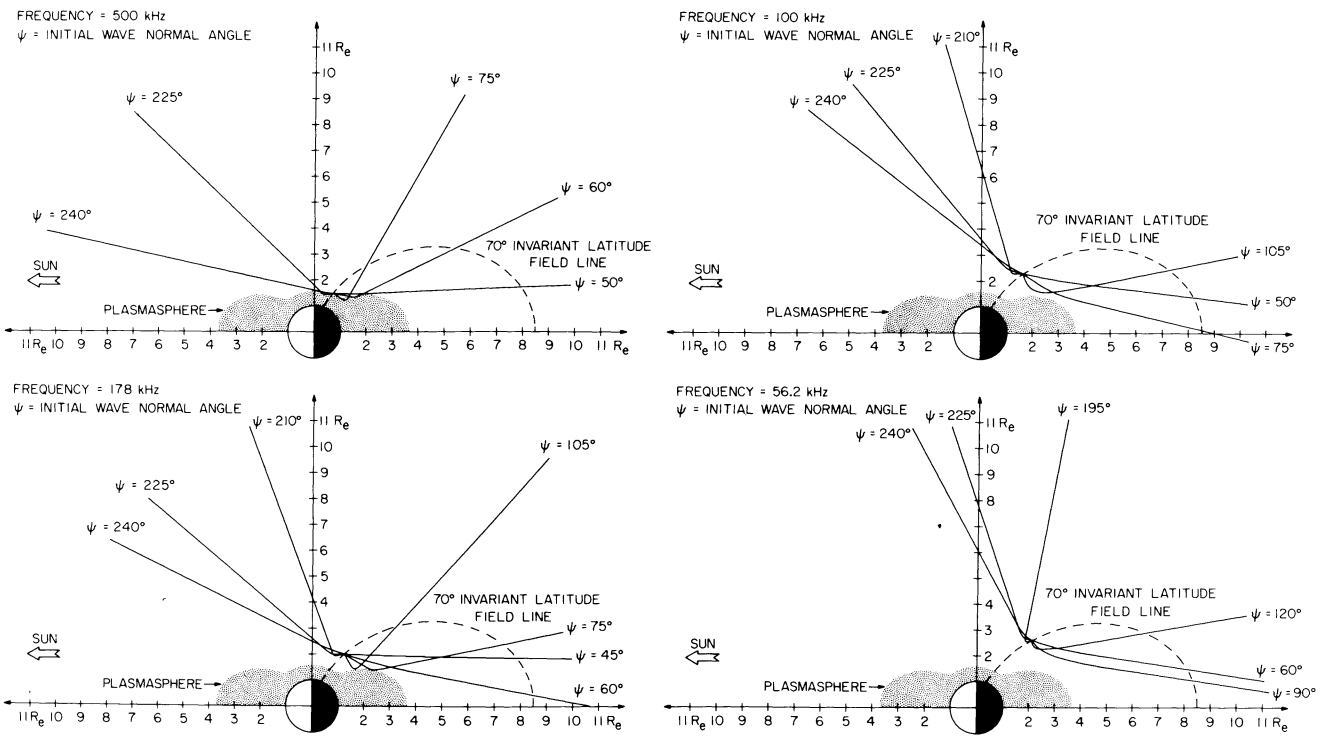

Fig. 12. Additional *R-X* mode ray tracing examples in the model II magnetosphere at 500, 178, 100, and 56.2 kHz. The source locations are the same as those used in Figure 11. Note the effect that a contracted plasmapause has on the angular extent of this radiation when this figure is compared to Figure 11. The contracted plasmapause allows the *R-X* radiation to propagate to the equator at lower altitude while the dayside distribution remains unchanged.

frequency range of the UHR noise the plasma frequency associated with the plasmapause is between 56.2 and 100 kHz. The plasmapause density of 100 cm^{-3} used in models I and II gives an electron plasma frequency of about 90 kHz, which is consistent with these observations. In Figure 9 the position of the plasmapause on the dayside is approximately 3.3 R_E at λ_m = 18.6°. The plasmapause (100-cm^{-3} density contour) in model II at λ_m = 18.6° is also 3.3 R_E. In Figure 9 on the nightside the plasmapause is at approximately 3.87 R_E at λ_m = 17.8°, which is halfway between the model I and II plasmapause positions.

Program Description

The ray tracing computer program used in this study was initially developed by *Shawhan* [1966, 1967*a*, *b*]. The program is based on a closed set of first-order differential equations in spherical polar coordinates derived by *J. Haselgrove* [1955]

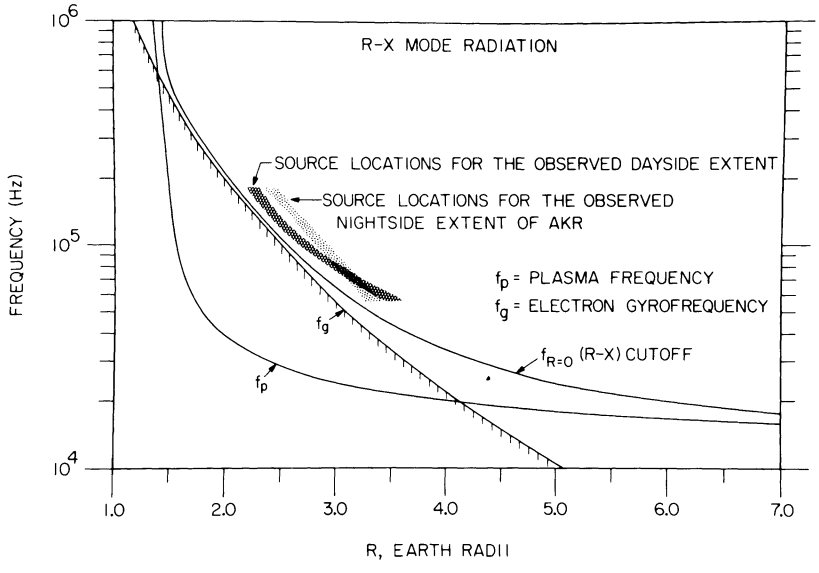

Fig. 13. Radial variation of the *R-X* cutoff frequency along the 70° invariant latitude magnetic field line in the model I or II magnetosphere. The cross-hatching indicates the source region determined from matching the dayside latitudinal cutoff of AKR to the *R-X* mode ray paths in the model I or II magnetosphere. The dot pattern indicates the *R-X* mode source region determined from the nightside latitudinal cutoff of AKR by using the model II magnetosphere.

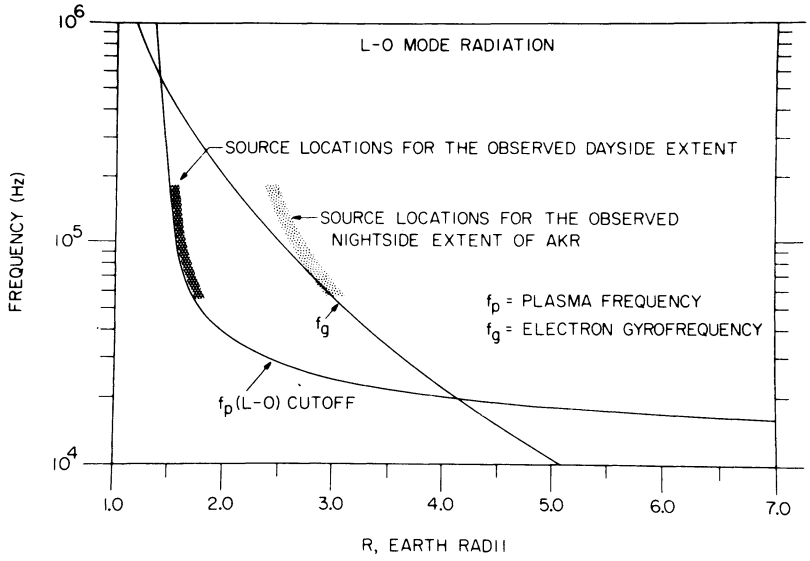

Fig. 14. Source regions in the midnight meridian (along a 70° invariant latitude field line) which produce rays of frequencies 178–56.2 kHz in the *L-O* mode whose latitudinal cutoffs are consistent with the observed AKR angular distribution. The cross-hatching indicates the source region in model I or model II determined from only the dayside latitudinal cutoff of AKR. The dot pattern indicates the source region in model II determined from only the nightside latitudinal cutoff of AKR.

and *C. G. Haselgrove and J. Haselgrove* [1960]. The equations were specialized by *Shawhan* [1966] for ray tracing in a magnetic meridian for a model magnetosphere. The expressions for the phase index of refraction and its derivatives are from the cold plasma formulation by *Stix* [1962]. The behavior of a ray path is determined by the frequency of the wave, the initial wave normal angle, the initial latitude, the initial altitude, the propagation mode, and the magnetospheric model.

Ray Tracing Results

All ray tracing calculations and source locations presented here are in the noon-midnight meridian. Since the source of AKR at a particular frequency 'subtends a small angular size' [*Gurnett*, 1974], all rays at a particular frequency are assumed to emanate from a point source along a 70° invariant latitude field line. The 70° invariant latitude field line is used to be consistent with observations of actual AKR source locations made by *Alexander and Kaiser* [1976]. Each source location is assumed to emit electromagnetic radiation at all wave normal angles ψ. For any given source location, two specific wave normal directions will give the most extreme dayside and nightside latitudinal limits to the ray directions at large radial distances, all of the other wave normal angles giving intermediate ray directions. By varying the source latitude along the magnetic field line a unique altitude can be found for each frequency which will give a limiting ray direction in agreement with the observed dayside (or nightside) latitudinal limit. By performing this analysis as a function of frequency a unique determination can be obtained for the source altitude as a function of frequency which can be compared with the various theories for AKR generation.

To demonstrate some of the basic ray path effects involved in this analysis, Figure 11 shows *R-X* mode rays calculated in the model I magnetosphere (plasmapause *L* value of 4.6) for various selected wave normal angles. The wave normal angles shown include those which give the most extreme dayside and nightside latitudinal limits to the ray paths, as well as other rays at intermediate wave normal angles. The dayside latitudinal limits are in good agreement with what is qualitatively observed; the higher the frequency, the lower the magnetic latitude at which the radiation can be observed. Rays on the nightside penetrate the topside plasmapause to depths qualitatively consistent with those in Figure 9. These ray paths show that the plasmapause presents a refracting layer. The ray behavior (*R-X* mode) in the model II magnetosphere (plasmapause *L* value of 3.6) for the same source region is illustrated in Figure 12. The latitudinal extent of the dayside rays is the same as that for Figure 11, which shows that the dayside rays are relatively unaffected by the plasmapause. The substantial change in the angular distribution on the nightside demonstrates that the position of the plasmapause for this assumed source region strongly determines the latitudinal extent of the ray paths on the nightside of the earth. The smaller plasmapause has allowed the rays to propagate down to the equatorial plane on the nightside.

The assumed radial variation of the frequency of the *R-X* cutoff ($R = 0$) along a 70° invariant latitude field line in the model magnetospheres is illustrated in Figure 13. The $R = 0$ cutoff is the same for both plasma models because the size of the plasmasphere is not thought to affect the electron densities significantly at high latitudes. By adjusting the source altitude so that the limiting ray angles agree with the observed latitudinal limits of the angular distribution (within specified limits) a range of source altitudes can be found which would produce the observed angular distribution at each frequency. For instance, the crosshatched region in Figure 13 shows the relationship found between source altitudes and frequencies which would result in dayside *R-X* rays whose latitudinal limit at large radial distance agreed (to within ±5°) with the observed angular distributions on the dayside of the earth. On the dayside the source region is essentially identical for models I and II because of the previously mentioned insensitivity to the plasmapause location in this region. On the nightside of the earth the corresponding source region required to obtain agreement with the nighttime angular distribution is indicated by the dot pattern in Figure 13. This source region was calcu-

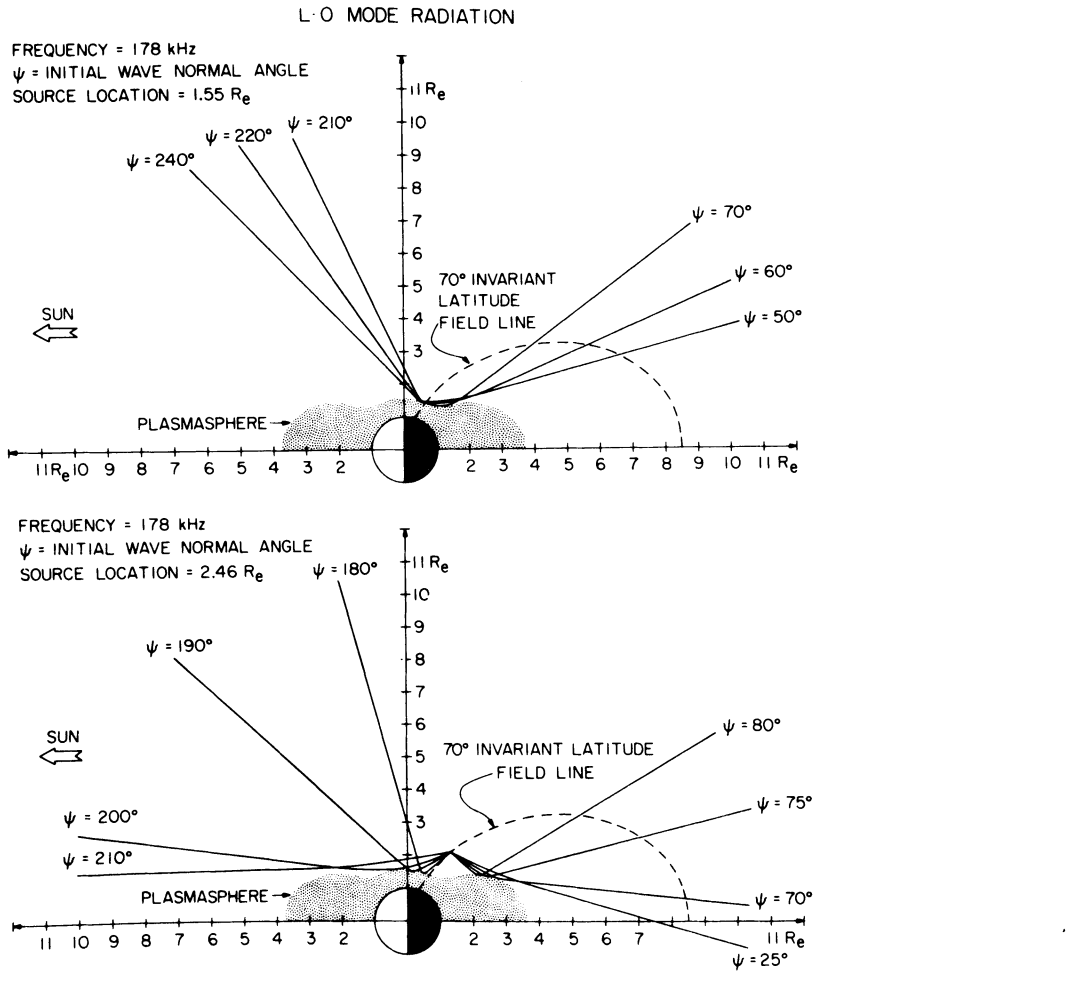

Fig. 15. *L-O* mode ray paths in the model II magnetosphere at 178 kHz. The top panel has a source location that lies within the cross-hatched region of Figure 14 and thus produces rays on the dayside whose latitudinal cutoffs are consistent with the observed angular distribution of AKR. The bottom panel has a source location from the dotted region of Figure 14 and produces rays on the nightside whose latitudinal cutoffs are consistent with the nightside extent of AKR at this frequency. Note that the dayside rays from such a source extend almost down to the dayside plasmapause. Angular distributions of this type are never observed on the dayside of the earth.

lated by using model II and is slightly different for model I (not shown) because of the dependence on the size of the nightside plasmapause.

The *L-O* mode radiation can propagate only in regions where the wave frequency is greater than the electron plasma frequency f_p. Since the electron plasma frequency is less than the $R = 0$ cutoff frequency in the frequency range where the AKR is observed, *L-O* mode radiation must be generated closer to the earth than the *R-X* mode to produce the same angular distribution. The ray tracing results for the *L-O* mode are summarized in Figure 14, which shows the computed source regions and their relationship to the electron plasma frequency. The crosshatched region again shows the source altitudes that produce *L-O* rays consistent with the observed dayside latitudinal limits of the AKR angular distribution. The dot pattern shows the corresponding source altitudes which produce *L-O* rays consistent with the observed nightside latitudinal limits. The source regions which account for the dayside and nightside angular distributions in Figure 14 are seen to be much further apart than the corresponding regions for the *R-X* rays in Figure 13. The origin of the inconsistency in the angular distribution of the dayside and nightside *L-O* rays is illustrated in the top panel of Figure 15. Source positions which give good agreement with the observed dayside latitudinal limits are shielded by the topside of the plasmapause on the nightside and never reach the equator at the low latitudes observed on the nightside of the earth. If the altitude of the source is moved up, as in the bottom panel of Figure 15, to account for the nightside observations, the rays penetrate to much lower latitudes than they do on the dayside of the earth.

Summary and Discussion

This study has shown that the intense kilometric radio emissions generated over the nightside auroral regions are beamed into a cone-shaped region whose axis of symmetry is tilted away from the magnetic axis of the earth, toward local evening, by about 20°. The solid angle of this emission cone increases systematically with increasing frequency, varying from approximately 1.1 sr at 56.2 kHz to approximately 3.5 sr at 178 kHz. Simultaneous measurements from two satellites show a good correlation between the radio emission intensities observed over a wide range of angular separations within the emission cone, indicating that the kilometric radiation source simultaneously illuminates the entire region within the emission cone with comparable intensities. A clear day-night asymmetry is observed in the propagation cutoffs at the plasma-

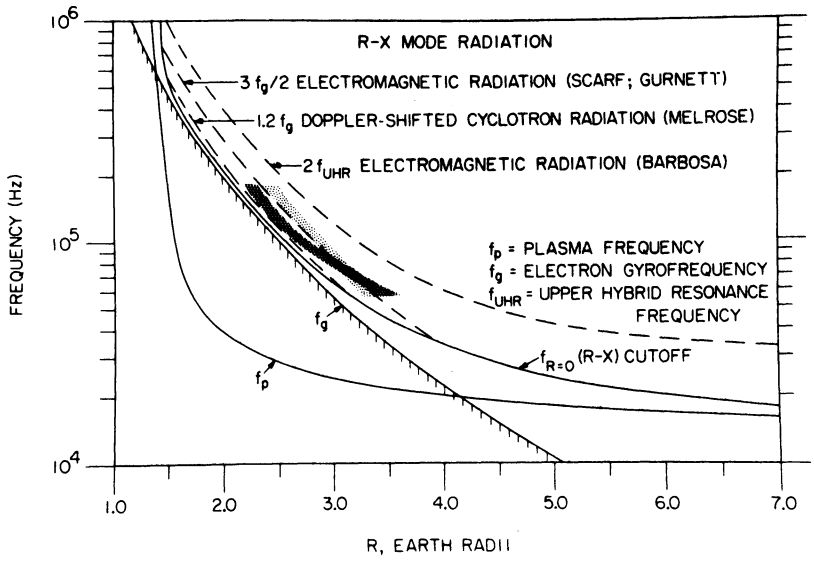

Fig. 16. Source locations (dashed lines) for three proposed *R-X* mode generation mechanisms as a function of emission frequency, shown in comparison to the AKR source regions determined from ray tracing calculations. Electromagnetic waves generated at $3f_g/2$ [*Scarf*, 1974; *Gurnett*, 1974] would originate from a region which produced an angular distribution qualitatively consistent with that observed for AKR. Radiation at $1.2f_g$ [*Melrose*, 1976] and $2f_{UHR}$ [*Barbosa*, 1976] would not produce a consistent angular distribution.

pause, with sharp cutoffs on the nightside of the earth and no corresponding cutoff on the dayside.

In an attempt to understand the essential features of the angular distribution of the AKR a detailed study of ray paths was performed for various source positions along a magnetic field line at 70° invariant latitude. Two magnetospheric density models were used which reflected the range of plasmapause locations encountered during moderately disturbed and disturbed magnetic conditions. By adjusting the altitude of the source to agree with the observed latitudinal cutoffs of the emission cone on the dayside and nightside of the earth a range of source positions were obtained as a function of frequency. These calculations were performed for both the *R-X* and the *L-O* mode of propagation.

In interpreting these ray tracing results it is essential that the uncertainties and limitations of the ray tracing analysis be carefully examined. Three main areas of uncertainty can be identified: (1) the spatial distribution of the source, (2) the distribution of initial wave normal angles, and (3) the plasma density models. For the ray tracing results presented we have assumed that the source is a point source at each frequency. Although height variations of the source have been considered, no attempt has been made to consider a spatially extended source in MLT and latitude. The assumption of a point source is primarily due to the lack of adequate information on the actual spatial extent of the source in local time and latitude. Conceptually, one can visualize the angular distribution from a spatially extended source by superposing the ray paths from an equivalent distribution of point sources. Even though very extreme source locations have been observed in some situations (at radial distances greater than 7 R_E and in the polar cusp on the dayside of the earth), these extreme cases are believed to occur so infrequently that they do not make a significant contribution to the long-term average results presented in this study. From our previous direction finding studies [*Kurth et al.*, 1975] and from those of *Kaiser and Stone* [1975] it is clear that the dominant component of the high-intensity ($\geq 2 \times 10^{-16}$ W m^{-2} Hz^{-1} at 30 R_E) kilometric radiation comes from the nightside auroral regions. The fact that the ray tracing calculations for the *R-X* mode fit the average features of the angular distribution is considered further confirmation that the source is relatively small and that the average position is on the nightside relatively close (2.25–3.5 R_E) to the earth.

The ray tracing results presented have assumed that the radiation is generated over a wide range of wave normal angles. This assumption is justified mainly by the fact that the radiation appears to be almost uniformly distributed throughout the emission cone. If the radiation were generated within a narrow range of wave normal angles, then the angular distribution should be sharply peaked at a well-defined angle with respect to the local magnetic field, such as it is for the decametric radiation generated by Jupiter's moon Io. Even when the possible smearing effect caused by a spatially extended source is taken into consideration, it seems unlikely that the near-uniformity of the illumination throughout the emission cone can be explained if the wave normal direction is sharply limited to a narrow range of angles. This conclusion is confirmed by the ray tracing calculations of *Jones and Grard* [1976], who assumed that the wave normal directions are either parallel or perpendicular (within 10°) to the magnetic field. Their calculations give quite different limiting ray paths from our results and do not appear to be in good agreement with the observed angular distributions. Since virtually all theories of the terrestrial kilometric and Jovian decametric radiation lead to a preferred wave normal direction for the emitted radiation, these conclusions may appear to conflict with the theoretical expectations. However, this difficulty could be explained if there is a substantial amount of scattering in the source region which could act to spread the angular distribution of the emitted radiation. The presence of such scattering would be entirely consistent with the large density fluctuations typically observed in the auroral electron precipitation at high altitudes.

Probably the primary uncertainty in the ray tracing comparisons with the observed angular distributions is the electron density models used in these calculations. Although the den-

sity models used are believed to be reasonably representative on the basis of certain general considerations, such as matching the observed ionospheric densities and scale heights at low altitudes and the low densities (<1 cm^{-3}) at large distances in the magnetotail, there are essentially no adequate density measurements at intermediate radial distances (from about 2 to 10 R_E) over the polar regions to confirm these models. The effect of errors in the density model on the ray tracing results is quite different for the two modes of propagation. In the region of primary interest from about 2.0 to 3.5 R_E one can be reasonably confident that the plasma frequency is substantially less than the electron gyrofrequency ($f_p^- \ll f_g^-$). Under these conditions the index of refraction for the *R-X* mode (and the $R = 0$ cutoff, as in Figure 13) is mainly determined by the magnetic field strength and is relatively independent of the plasma density. The ray paths for the *R-X* mode are therefore relatively insensitive to changes in the plasma density model. For the *L-O* mode of propagation, however, the propagation cutoff occurs at the local plasma frequency, and the ray paths and source altitudes are very sensitive to changes in the plasma density. Even small horizontal gradients, which change the slope of the constant density contours, cause marked changes in the angle of reflection and the angular distribution at large radial distances. Indirectly, the sensitivity of the *L-O* mode to horizontal gradients in the plasma density, which must almost certainly occur near the auroral field lines, provides additional evidence that the AKR is not propagating in the *L-O* mode. As was mentioned earlier, the dayside latitudinal cutoff at $\lambda_m = 65° \pm 10°$ is very sharp and consistent. Considering the probable variability of the horizontal gradients in the plasma density near the reflection point, it is hard to see how this dayside cutoff can be so stable and consistent if the radiation is emitted in the *L-O* mode. In contrast, the magnetic control of the *R-X* mode provides a relatively stable reflecting surface (at the $R = 0$ cutoff) which would result in a nearly constant limiting ray path at a given frequency, independent of the electron density variations near the reflecting region.

From these ray tracing considerations it is our conclusion that the *R-X* mode provides the best and most consistent agreement with the observed angular distribution of the AKR. Because of the many uncertainties involved in the detailed ray tracing models and the mechanism by which this radiation is generated it is obvious that this conclusion cannot be considered firm. Direct measurements of the polarization or other techniques are needed to provide the final determination of the polarization. However, it is of interest to note that the Jovian decametric radiation, which is generally thought to be equivalent to the intense terrestrial kilometric radiation, has been determined by *Warwick and Dulk* [1963] to be emitted in the *R-X* mode, in agreement with the conclusions of this study.

The limitations placed on the source regions of AKR which are illustrated in Figures 13 and 14 can be used to test the validity of proposed emission mechanisms. Since the ray tracing calculations favor the generation of AKR in the *R-X* mode, we will consider only those mechanisms proposed by *Scarf* [1974], *Gurnett* [1974], *Melrose* [1976], and *Barbosa* [1976]. *Scarf* [1974] and *Gurnett* [1974] proposed that planetary emissions such as AKR may be produced from electrostatic plasma instabilities (set up by precipitating electrons) that couple into electromagnetic waves at $3f_g/2$. As is shown in Figure 16, electromagnetic waves at $3f_g/2$ would originate from a region which produced an angular distribution qualitatively consistent with that observed for AKR. Another mechanism which is gyro related was proposed by Melrose. In his theory, *R-X* cyclotron radiation from precipitating electrons is Doppler-shifted upward in frequency, above the $R = 0$ cutoff, so that the radiation can escape. For an energy of 10 keV, typical of the auroral electron precipitation, the Doppler shift is about 20%, which would produce radiation at $f = 1.2f_g^-$. The source region for the Doppler-shifted cyclotron radiation mechanism would then correspond to frequencies of about $1.2f_g^-$ along a 70° invariant latitude field line. As is illustrated in Figure 16, radiation at $f = 1.2f_g^-$ would originate from a region below the region determined by our ray tracing analysis. Electron energies of at least 50 keV are needed to produce Doppler shifts sufficiently large to be in agreement with the observed angular distribution. Although electrons with energies greater than 50 keV are occasionally observed in the auroral electron precipitation, these electrons do not constitute a very large fraction of available energy and would not be expected to play a significant role in the generation of the intense AKR. *Barbosa*'s [1976] mechanism produces *R-X* radiation near twice the UHR frequency ($2f_{UHR}$). Radiation at $2f_{UHR}$ originates from a region at larger radial distances than those indicated by the dot pattern of Figure 16. Much larger emission cones than those observed for AKR would result from *R-X* mode radiation of $2f_{UHR}$ in the model magnetospheres presented in this study.

CONCLUSIONS

Analysis of spacecraft data from Hawkeye 1, Imp 6, and Imp 8 has led to the following conclusions concerning the propagation characteristics of AKR:

1. AKR in the northern hemisphere is beamed into a cone-shaped region whose solid angle increases with increasing frequency, varying from approximately 1.1 sr at 56.2 kHz to approximately 3.5 sr at 178 kHz.
2. There is simultaneous illumination with nearly constant intensities over the entire solid angle.
3. The symmetry axis of the emission cone is tilted toward local evening by about 20° with respect to the magnetic axis of the earth.
4. There is a day-night asymmetry in the topside plasmapause cutoffs, with sharp cutoffs on the nightside of the earth and no corresponding cutoff on the dayside.

Ray tracing calculation for the escaping modes *R-X* and *L-O* using two magnetospheric density models leads to the following conclusions:

5. Variability in the size of the nightside plasmapause can account for the nightside variability in the angular distribution of AKR, as is suggested by Figures 2, 3, 4, and 5.
6. Rays in either of the *R-X* or *L-O* modes exhibit the day-night asymmetry in the topside plasmapause cutoffs.
7. The angular distribution of AKR can best be reproduced from low-altitude source regions (from 2 to 3.5 R_E) in the nighttime auroral zone if the emission is in the *R-X* mode.

Acknowledgments. The research at the University of Iowa was supported by the National Aeronautics and Space Administration through grants NGL-16-001-002 and NGL-16-001-043, contracts NAS1-11257 and NAS1-13129 with Langley Research Center, and contracts NAS5-11074 and NAS5-11431 with Goddard Space Flight Center; by the Office of Naval Research; and by the Atmospheric Sciences Section of the National Science Foundation.

The Editor thanks J. K. Alexander and W. Bernstein for their assistance in evaluating this paper.

REFERENCES

Ackerson, K. L., and L. A. Frank, Correlated satellite measurements of low-energy electron precipitation and ground-based observations

of a visible auroral arc, *J. Geophys. Res., 77,* 1128, 1972.
Alexander, J. K., and M. L. Kaiser, Terrestrial kilometric radiation, 1, Spatial structure studies, *J. Geophys. Res., 81,* 5948, 1976.
Barbosa, D. D., Electrostatic mode coupling at $2\omega_{UH}$: A generation mechanism for auroral kilometric radiation, Ph.D. dissertation, Dep. of Phys., Univ. of Calif., Los Angeles, 1976.
Benson, R. F., Source mechanism for terrestrial kilometric radiation, *Geophys. Res. Lett., 2,* 52, 1975.
Carpenter, D. L., Whistler evidence of a 'knee' in the magnetospheric ionization density profile, *J. Geophys. Res., 68,* 1675, 1963.
Dunckel, N., B. Ficklin, L. Rorden, and R. A. Helliwell, Low-frequency noise observed in the distant magnetosphere with Ogo 1, *J. Geophys. Res., 75,* 1854, 1970.
Gurnett, D. A., The earth as a radio source: Terrestrial kilometric radiation, *J. Geophys. Res., 79,* 4227, 1974.
Gurnett, D. A., The earth as a radio source: The nonthermal continuum, *J. Geophys. Res., 80,* 2751, 1975.
Haselgrove, C. G., and J. Haselgrove, Twisted ray paths in the ionosphere, *Proc. Roy. Soc. London, 75,* 357, 1960.
Haselgrove, J., Ray theory and a new method for ray tracing, Report of Conference on the Physics of the Ionosphere, p. 355, Phys. Soc., London, 1955.
Jones, D., Mode-coupling of *z*-mode waves as a source of terrestrial kilometric and Jovian decametric radiation, submitted to *Astron. Astrophys.,* 1976.
Jones, D., and R. J. L. Grard, Propagation characteristics of electromagnetic waves in the magnetosphere, in *The Scientific Satellite Programme During the Magnetospheric Study,* edited by K. Knott and B. Battrick, p. 293, D. Reidel, Dordrecht, Netherlands, 1976.
Kaiser, M. L., and J. E. Alexander, Source measurements of terrestrial kilometric radiation obtained from lunar orbit, *Geophys. Res. Lett., 3,* 37, 1976.
Kaiser, M. L., and R. G. Stone, Earth as an intense planetary radio source: Similarities to Jupiter and Saturn, *Science, 189,* 285, 1975.
Kurth, W. S., M. M. Baumback, and D. A. Gurnett, Direction finding measurements of auroral kilometric radiation, *J. Geophys. Res., 80,* 2764, 1975.
Lin, R. P., The emission and propagation of ~40 keV solar flare electrons, *Solar Phys., 12,* 266, 1970.
Melrose, D. B., An interpretation of Jupiter's decametric radiation and the terrestrial kilometric radiation as direct amplified gyroemission, *Astrophys. J., 207,* 651, 1976.
Palmadesso, P., T. P. Coffey, S. L. Ossakow, and K. Papadopoulos, Generation of terrestrial kilometric radiation by a beam-driven electromagnetic instability, *J. Geophys. Res., 81,* 1762, 1976.
Scarf, F. L., A new model for the high-frequency decametric radiation from Jupiter, *J. Geophys. Res., 79,* 3835, 1974.
Shaw, R. R., and D. A. Gurnett, Electrostatic noise bands associated with the electron gyrofrequency and plasma frequency in the outer magnetosphere, *J. Geophys. Res., 80,* 4259, 1975.
Shawhan, S. D., VLF ray tracing in a model ionosphere, *Res. Rep. 66-33,* Dep. of Phys. and Astron., Univ. of Iowa, Iowa City, 1966.
Shawhan, S. D., A computer program for VLF ray tracing in a model ionosphere, *Res. Rep. 67-12,* Dep. of Phys. and Astron., Univ. of Iowa, Iowa City, 1967*a*.
Shawhan, S. D., Behavior of VLF ray paths in the ionosphere, *Res. Rep. 67-25,* Dep. of Phys. and Astron., Univ. of Iowa, Iowa City, 1967*b*.
Stix, T. H., *The Theory of Plasma Waves,* McGraw-Hill, New York, 1962.
Voots, G., D. A. Gurnett, and S.-I. Akasofu, Auroral kilometric radiation as an indicator of auroral magnetic disturbances, submitted to *J. Geophys. Res.,* 1976.
Warwick, J. W., and G. A. Dulk, Faraday rotation on decametric radio emissions from Jupiter, *Science, 145,* 380, 1963.

(Received September 13, 1976;
accepted January 27, 1977.)